Journal of Inorganic Biochemistry xxx (2016) xxx–xxx

Contents lists available at ScienceDirect

Journal of Inorganic Biochemistry

journal homepage: www.elsevier.com/locate/jinorgbio

Engineering nitric oxide synthase chimeras to function as NO dioxygenases

Zhi-Qiang Wang [a,*,1], Mohammad Mahfuzul Haque [b,1], Katherine Binder [b], Manisha Sharma [b], Chin-Chuan Wei [c], Dennis J. Stuehr [b,**]

[a] Department of Chemistry and Biochemistry, Kent State University Geauga, Burton, OH 44021, United States
[b] Department of Pathobiology, Lerner Research Institute, Cleveland Clinic, Cleveland, OH 44195, United States
[c] Department of Chemistry, Southern Illinois University Edwardsville, Edwardsville, IL 62026, United States

ARTICLE INFO

Article history:
Received 12 November 2015
Received in revised form 10 March 2016
Accepted 12 March 2016
Available online xxxx

Keywords:
Chimera
Electron transfer
Kox
Heme reduction
Catalysis
Stopped-flow

ABSTRACT

Nitric oxide synthases (NOSs) catalyze a two-step oxidation of L-arginine to form nitric oxide (NO) and L-citrulline. NOS contains a N-terminal oxygenase domain (NOSoxy) that is the site of NO synthesis, and a C-terminal reductase domain (NOSred) that binds nicotinamide adenine dinucleotide phosphate (NADPH), flavin adenine dinucleotide (FAD), and flavin mononucleotide (FMN) and provides electrons to the NOSoxy heme during catalysis. The three NOS isoforms in mammals inducible NOS (iNOS), neuronal NOS (nNOS), and endothelial NOS (eNOS) share high structural similarity but differ in NO release rates and catalytic properties due to differences in enzyme kinetic parameters. These parameters must be balanced for NOS enzymes to release NO, rather than consume it in a competing, inherent NO dioxygenase reaction. To improve understanding, we drew on a global catalytic model and previous findings to design three NOS chimeras that may predominantly function as NO dioxygenases: iNOSoxy/nNOSred (Wild type (WT) chimera), V346I iNOSoxy/nNOSred (V346I chimera) and iNOSoxy/S1412D nNOSred (S1412D chimera). The WT and S1412D chimeras had higher NO release than the parent iNOS, while the V346I chimera exhibited much lower NO release, consistent with expectations. Measurements indicated that a greater NO dioxygenase activity was achieved, particularly in the V346I chimera, which dioxygenated an estimated two to four NO per NO that it released, while the other chimeras had nearly equivalent NO dioxygenase and NO release activities. Computer simulations of the global catalytic model using the measured kinetic parameters produced results that mimicked the measured outcomes, and this provided further insights on the catalytic behaviors of the chimeras and basis of their increased NO dioxygenase activities.

1. Introduction

Nitric oxide synthases (NOSs) are flavo-heme enzymes that catalyze a stepwise oxidation of L-arginine (Arg) to form nitric oxide (NO) and L-citrulline [1–6]. The overall biosynthetic reaction consumes 1.5 nicotinamide adenine dinucleotide phosphate (NADPH) and 2 O_2 and involves two steps: the first being Arg hydroxylation to form N-hydroxy-L-Arg (NOHA), and the second being NOHA oxidation to form citrulline and NO (Scheme 1). NOSs are homodimeric enzymes [5,7,8], with each monomer containing an N-terminal oxygenase domain that binds Fe-protoporphyrin IX (heme), the substrate Arg, and the cofactor 6R-tetrahydrobiopterin (H_4B) [9–11], and a C-terminal flavoprotein domain that binds flavin adenine dinucleotide (FAD), flavin mononucleotide (FMN), and NADPH [12–15], with the two domains being linked by a central calmodulin (CaM) binding motif [6,16,17]. Neuronal NOS (nNOS) and endothelial NOS (eNOS) are reversibly activated by binding CaM in the presence of Ca^{2+}. Whereas iNOS binds CaM regardless of the Ca^{2+} concentration and is continuously active [1,2,16,18]. The enzyme heme is ligated to a cysteine

Abbreviation: Arg, L-arginine; DTT, dithiothreitol; NO, nitric oxide; EPPS, 4-(2-hydroxyethyl)-1-piperazinepropanesulfonic acid; NOHA, N^{ω}-hydroxy-L-arginine; H_4B, (6R)-5, 6, 7, 8-tetrahydro-L-biopterin; FMN, flavin mononucleotide; FAD, flavin adenine dinucleotide; NADPH, nicotinamide adenine dinucleotide phosphate; NED, N-1-naphthylethylenediamine dihydrochloride; LDH, lactate dehydrogenase; SEITU, S-ethylisothiourea; NOS, nitric oxide synthase; iNOS, inducible nitric oxide synthase; nNOS, neuronal nitric oxide synthase; eNOS, endothelial nitric oxide synthase; NOSoxy, the oxygenase domain of nitric oxide synthase; NOSred, the reductase domain of nitric oxide synthase; iNOS fl, the full length of inducible nitric oxide synthase; Fe^{II}, ferrous heme species; Fe^{III}, ferric heme species; $Fe^{II}O_2$, ferrous oxy species; $Fe^{III}NO$, ferric NO species; $Fe^{II}NO$, ferrous NO species; k_r, ferric heme reduction rate; k_{ox}, ferrous heme-NO oxidation rate; k_d, ferric heme-NO dissociation rate; k_{on}, NO association to the ferric enzyme; k_{cat1}, catalytic rate constant of Arg hydroxylation; k_{cat2}, catalytic rate constant of NOHA oxidation; BSA, bovine serum albumin; SOD, superoxide dismutase.

* Corresponding author.
** Correspondence to: D. J. Stuehr, Department of Pathobiology NC-22, Lerner Research Institute, Cleveland Clinic Foundation, 9500 Euclid Avenue, Cleveland, OH 44195, United States.
E-mail addresses: zwang3@kent.edu (Z.-Q. Wang), stuehrd@ccf.org (D.J. Stuehr).
[1] Both authors contributed equally to this work.

http://dx.doi.org/10.1016/j.jinorgbio.2016.03.002
0162-0134/

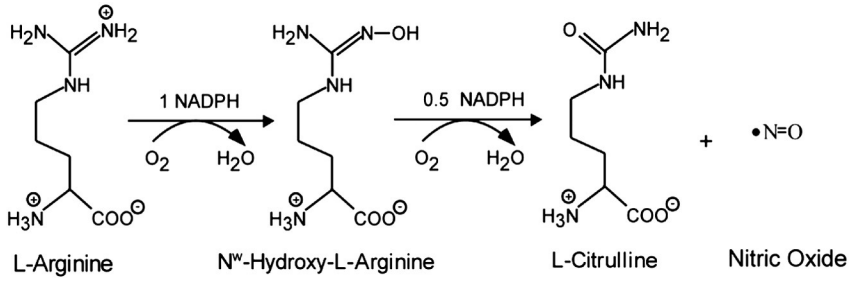

Scheme 1. The two steps of NO synthesis.

thiolate and acts in conjunction with H_4B to catalyze a reductive activation of molecular oxygen in both steps of NO synthesis [16,19–21].

Three mammalian NOS isozymes have been characterized: neuronal NOS (nNOS), inducible NOS (iNOS) and endothelial NOS (eNOS) [1,2,18,22–30]. Each is distinguished by its tissue location, regulation, and function [31–37]. Rates of NO synthesis (release) also differ among the mammalian NOS with the rank order being iNOS > nNOS ≫ eNOS. Numerous results show that their catalytic differences are predominantly due to the differences in three main kinetic parameters: The rates of ferric heme reduction (k_r, k_r', k_r") ferric heme-NO dissociation (k_d), and ferrous heme–NO oxidation (k_{ox}) (Fig. 1) [23,24,38–41]. In both the Arg hydroxylation and NOHA oxidation reactions of NO synthesis, the NOS ferric heme first accepts an electron from the reductase domain (k_r & k_r" in Fig. 1) to form the heme-dioxy species ($Fe^{II}O_2$, Fig. 1), which is unreactive toward Arg or NOHA. An electron is then provided by cofactor H_4B to form the ferric peroxy intermediate, and this H_4B-mediated electron transfer is rate limiting for the subsequent catalytic steps in Arg hydroxylation and in NO production from NOHA (k_{cat1}, k_{cat2}, Fig. 1) [19,21,42–44]. Practically all of the newly-generated NO binds to the NOS ferric heme to form $Fe^{III}NO$ before exiting the enzyme. The dissociation of this ferric heme–NO complex (k_d) is part of a "productive cycle" that releases NO and is essential for NOS bioactivity. Conversely, the attached reductase domain (NOSred) can reduce the ferric heme–NO complex (k_r'"; k_r'" = k_r) [41] to channel the enzyme into an NO dioxygenase "futile cycle" that ultimately generates nitrate in place of NO. Together, the productive and futile cycles create a global kinetic model for NOS catalysis. The global catalytic model reveals how the k_r, k_{cat}, k_d, and k_{ox} parameters must be balanced in order for NOS enzymes to release the NO that they make, and to minimize destruction of the NO in the futile dioxygenase pathway. Interestingly, the set points for k_r, k_{cat}, k_d, k_{ox} vary among NOS enzymes [27,29,41,45] and give each NOS a unique catalytic profile, possibly to aid their specific functions in biology [29].

NO biosynthesis by NOS enzymes is rate-limited by k_r (i.e., k_r, k_r', k_r" limit the rate of $Fe^{III}NO$ formation in Fig. 1). Because the electron transfer from two-electron reduced (hydroquinone) FMN ($FMNH_2$) to the heme is rate-limiting, it likely nullifies the importance of any Fe^{II}/Fe^{III} thermodynamic differences that may exist among the various Fe^{III} species. But increasing k_r also makes the enzyme partition more into the futile cycle (k_r'", Fig. 1), which diminishes the proportion of NO released and increases the extent of NO dioxygenase activity and nitrate production (Fig. 1). In fact, the global kinetic model predicts that each NOS has an optimal k_r setting for its NO release rate, above which the NO release will fall and the NO dioxygenase activity will reciprocally increase [29].

Some of the protein features in NOS that help determine set points for the k_r, k_{cat}, k_d, and k_{ox} kinetic parameters have been identified [23,24,39,43,46]. In native enzymes, the identity of the NOS reductase domain appears to determine the k_r value [39,47], with rank order (fast to slow) nNOS > iNOS > eNOS, while the NOS oxygenase domain primarily determines the k_{ox} and k_d settings [29], with rank orders for k_{ox} being iNOS > eNOS > nNOS, and for k_d being nNOS > eNOS > iNOS. Our studies indicate that nNOS evolved a near optimal k_r setting for its NO release, whereas eNOS and iNOS have sub-optimal k_r rates [23,24,29,48,49]. Accordingly, a point mutation (S1412D) that mimics Akt-dependent Ser phosphorylation in the C-terminal region of nNOS increased it's heme reduction rate k_r, but also caused a lower NO release rate [50–53], consistent with it's k_r going beyond the optimal setting. This relationship was later confirmed and expanded in a study with several nNOS mutants [30].

Regarding the control of k_d, there is a naturally-occurring Ile present in the heme pocket opening in bacterial NOS enzymes that restricts

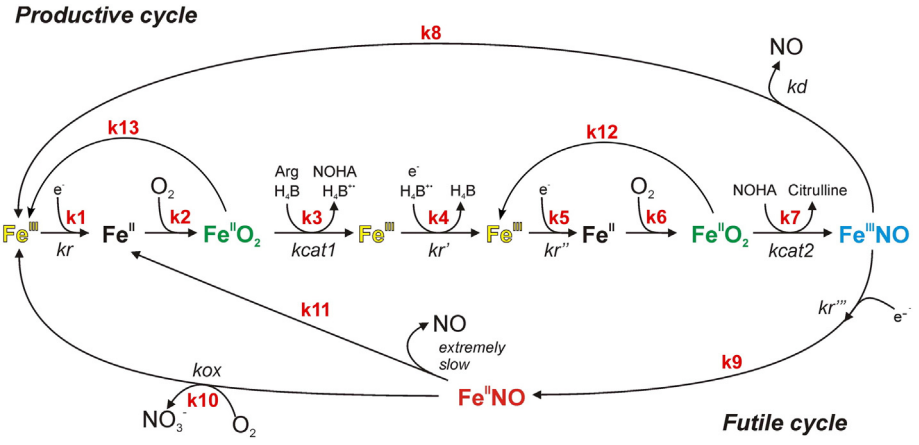

Fig. 1. Global kinetic model for NOS enzymes. During steady state catalysis, NOS molecules engage in a productive cycle that releases NO and in a futile NO dioxygenase cycle that releases nitrate. Reduction of ferric enzyme to ferrous (k_r) enables the heme to bind O_2 and initiate catalytic reactions, k_{cat1} and k_{cat2} in concert with donation of a second electron from H_4B cofactor, that converts the $Fe^{II}O_2$ species and generates products in both the Arg hydroxylation and NOHA oxidation reactions, respectively. After NO is made a ferric heme–NO complex (Fe^{III}—NO) forms, which can either release NO (k_d) or become reduced (k_r'") to generate a ferrous heme–NO complex (Fe^{II}—NO), which dissociates extremely slowly and instead regenerates the active ferric enzyme by reacting with O_2 in a dioxygenase reaction (k_{ox}).

Please cite this article as: Z.-Q. Wang, et al., Engineering nitric oxide synthase chimeras to function as NO dioxygenases, J. Inorg. Biochem. (2016), http://dx.doi.org/10.1016/j.jinorgbio.2016.03.002

newly-made NO from exiting the distal heme pocket, and also restricts small molecule (i.e., O_2 and NO) entrance into the heme pocket, as compared to the animal NOS enzymes, which have the smaller Val in place of Ile at this position. Thus, incorporating the V346I substitution into iNOS decreased its k_d about 3-fold, decreased its affinity toward binding external NO [49,54], and also increased the extent of it's geminate or near-geminate heme-NO rebinding, as demonstrated in a laser flash photolysis study of the enzyme heme–NO complex [55].

We took advantage of this knowledge described above to create three NOS chimeras that were specifically engineered to be better NO dioxygenases: iNOSoxy/nNOSred (WT chimera), iNOSoxy/S1412D nNOSred (S1412D chimera), and V346I iNOSoxy/nNOSred (V346I chimera). The rationale for using nNOSred is that it has the fastest k_r among the three NOS, and so should cause the greatest fraction of enzyme to partition into the futile NO dioxygenase cycle, which depends on k_r''' (k_r''' was measured to be equivalent in rate to k_r) [41] (see Fig. 1). The S1412D mutation was added in an attempt to further speed heme reduction and thus increases enzyme partitioning into the futile cycle. The rationale for using iNOSoxy is that its k_{ox} parameter is the fastest among the three NOS, and is faster than k_r, which should allow the enzyme to pass quickly through the futile cycle without accumulating as the ferrous heme-NO species, which otherwise would lower the overall catalytic cycling. The V346I mutation was added to slow k_d and prolong the lifetime of the $Fe^{III}NO$ product species, and thus give it more chance to become reduced and partition into the futile cycle (the productive/futile partitioning ratio is determined by k_r'''/k_d see Fig. 1).

We characterized the chimeras regarding their steady-state catalytic activities, heme reduction rates, and NO versus nitrate production, and then performed computer simulations using our global catalytic model [18,27,29,41,45,56] and both measured and reported kinetic values, to understand the behaviors of the three chimeras. The results indicate that they all gained in NO dioxygenase activity, and that the V346I chimera is a predominant NO dioxygenase, all generally consistent with the computer modeling. Our study provides a better understanding of NOS catalysis and it's protein structure–function relationships, regarding how NOS kinetic parameters are regulated and help balance coincident NO release and NO dioxygenase activities.

2. Materials and methods

2.1. Materials

All reagents and materials were obtained from Aldrich, Alexis, Sigma-Aldrich, or sources described previously [45,49,57].

2.2. Constructing NOS chimeras

The oxygenase domain of nNOS was replaced with the oxygenase domain of iNOS using NdeI restriction site at 5′-end and KpnI site (generated by site directed mutagenesis) at 3′-end (Fig. 2). Chimeras contain a 6-His tag at N-terminal and the CaM binding site from nNOS. Mutations (bold) and their corresponding oligonucleotides were as follows: S1412D (sense) 5′-CTT AGA TCT GAG **GAC** ATC GCC TTC ATC GAA-3′; S1412D (antisense) 5′-TTC GAT GAA GGC GAT **GTC** CTC AGA TCT AAG-3′; V346I (sense) 5′-TAT GCA CTG CCT GCC **ATT** GCC AAC ATG CTA-3′; V346I (antisense) 5′-TAG CAT GTT GGC **AAT** GGC AGG CAG TGC ATA-3′. Restriction digestions, cloning, and bacterial growth were performed using standard procedures. Transformations were done using a TransformAid bacterial transformation kit (ThermoFisher Scientific). Oligonucleotides used to construct site-directed mutants in nNOS were obtained from Integrated DNA Technologies (Coralville, IA). Site-directed mutagenesis was done using a QuikChange XL site-directed mutagenesis kit (Agilent Technologies). The hybrid constructs and mutants were confirmed by DNA sequencing at the Cleveland Clinic Genomics Core.

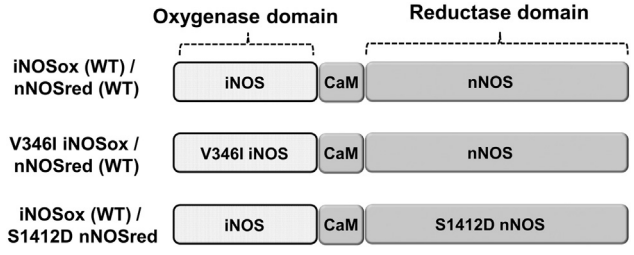

Fig. 2. Cartoon showing the chimeric proteins used in this study. All chimeric proteins are comprised of oxygenase domain from iNOS (iNOSoxy) and reductase domain from nNOS (nNOSred) that also contains the nNOS calmodulin (CaM) binding domain.

2.3. Protein expression and purification

Three chimeras, along with wild type iNOS with a six-histidine tag were each overexpressed in *E. coli* BL21(DE3) strain using pCWori vector and purified as reported previously by sequential Ni^{2+}-nitrilotriacetate (NTA) chromatography and CaM-sepharose affinity column [18,23,45,49,58–60]. NOS concentrations were determined from the 444 nm absorbance of the ferrous–CO complex, using an extinction coefficient 74 mM^{-1} cm^{-1} [61]. Buffer used for all experiments was 40 mM 4-(2-hydroxyethyl)-1-piperazinepropanesulfonic acid (EPPS, pH 7.6) containing 250 mM NaCl and 10% glycerol.

2.4. UV–Vis spectra measurement

Spectra of chimeras in the presence of 10 mM Arg and 20 μM H_4B were recorded at room temperature on Shimadzu UV-2410PC spectrophotometer (Shimadzu Corp., Tokyo, Japan). After addition of small amount of dithionite to the samples and bubbling with CO, the ferrous CO complex was measured. Spectra were also taken after adding 31 mM imidazole to the purified proteins.

2.5. NO synthesis and NADPH oxidation rates

Steady-state rates of NO release were determined by the spectrophotometric oxyhemoglobin assay using a difference extinction coefficient of 38 mM^{-1} cm^{-1} for the oxyhemoglobin to methemoglobin transition at 401 nm [26,45,58,60]. Sample solutions contained 0.1 μM NOS enzyme, 4 μM H_4B, 2 mM Arg, 0.3 mM DTT, 0.1 mg/ml bovine serum albumin (BSA), 10 U/ml superoxide dismutase (SOD), 346 U/ml catalase, 10 μM oxyhemoglobin, 4 μM FMN and FAD, 0.2 mM EDTA, 0.7 mM $CaCl_2$ and 12.5 μg/ml CaM. Reactions were initiated by adding NADPH (100 μM final concentration), and the absorbance change at 401 nm was recorded at room temperature or at 10 °C. For the NADPH oxidation rate measurements we used an extinction coefficient of 6.22 mM^{-1} cm^{-1} at 340 nm. In some cases 250 μM NOHA or 2 mM S-ethylisothiourea (SEITU) were added to the reaction solution in place of Arg.

2.6. Rates of heme reduction

The kinetics of ferric heme reduction was determined at 10 °C as described previously [18,26,30,58,59,62]. Reactions were carried out in a Hi-Tech Scientific KinetAsyst SF-61 DX2 stopped-flow apparatus equipped for anaerobic work and coupled to a diode array detector (Hi-Tech Scientific, Salisbury, UK). Reactions were initiated by rapidly mixing anaerobic ferric enzyme solutions containing ~10 μM NOS, 100 μM H_4B, 6 mM Arg, 0.4 mM Dithiothreitol (DTT), 1 mM EDTA, 10 mM $CaCl_2$ and 12.5 μg/ml CaM with an anaerobic CO-saturated buffer solution containing 100 μM NADPH. Heme reduction was determined by the absorbance increase at 444 nm due to formation of the ferrous–CO complex, which occurs following an initial absorbance decrease at

Please cite this article as: Z.-Q. Wang, et al., Engineering nitric oxide synthase chimeras to function as NO dioxygenases, J. Inorg. Biochem. (2016), http://dx.doi.org/10.1016/j.jinorgbio.2016.03.002

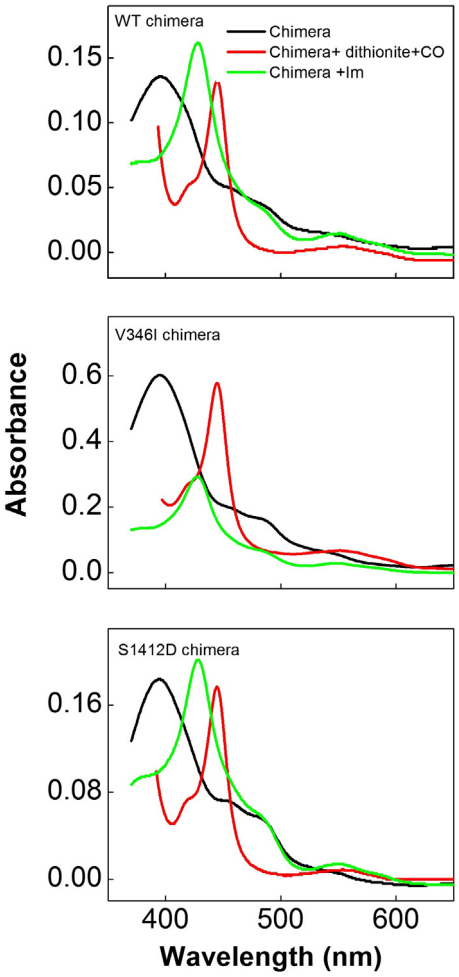

Fig. 3. Spectral properties of chimeric NOS enzymes. Spectra were recorded in the presence of 10 mM Arg and 20 μM H_4B for the ferric enzymes (black lines), the ferric-imidazole species (green lines), and the ferrous–CO complexes (red lines).

444 nm due to flavin reduction by NADPH. Rates were determined after fitting the absorbance change to a bi-exponential equation.

2.7. Nitrite and nitrate production in NADPH-driven reactions

90 μl 6–15 nM enzyme solutions containing 20 μM H_4B, 3 mM Arg, 0.3 mM DTT, 0.1 mg/ml BSA, 10 U/ml SOD, 346 U/ml catalase, 4 μM FMN and FAD and 12.5 μg/ml CaM were added into 96-well microplate and incubated on ice for 30 min. The reaction was initiated by adding 10 μl 10 mM NADPH. After having reacted for 30 min in 37 °C incubator, 10 μl 15 mM SEITU was added to each well to stop the reaction. Excess NADPH was consumed by the addition of 10 U/ml lactate dehydrogenase (LDH) and 10 mM sodium pyruvate. Nitrite was detected by measuring the absorbance difference at 550 and 650 nm using a microplate reader, after adding Griess reagent (0.1% NED (N-1-napthylethylenediamine dihydrochloride) solution and 1% sulfanilamide in 4.25% H_3PO_4) to each well. Nitrite productions were then quantitated based on nitrite solutions standard curve [29,49,63,64]. Total amount of nitrite plus nitrate was determined using a similar method except adding nitrate reductase (0.1 U/ml) and incubating the samples for extra 2 h at 37 °C before the addition of LDH and sodium pyruvate [49]. Nitrate production was calculated by subtracting the nitrite amount from the total amount.

2.8. Simulations of product formation and enzyme distribution during NO synthesis

Computer simulations were based on the global kinetic model described in Fig. 1 and *were run* in Gepasi 3.30 as described earlier [24]. The simulations assume constant values for $[O_2] = 180$ μM and [NADPH] = 40 μM. Values of ferric heme reduction (k_r), ferrous heme-NO oxidation (k_{ox}), heme NO dissociation (k_d), catalytic rate constants (k_{cat1}, k_{cat2}) used for simulation are listed in tables. Experimentally observed oxidation rates (k_{ox}) for ferrous heme–NO complexes, which we derived at half air-saturated condition, were multiplied by a factor of 1.5 to get a full air-saturated condition, based on our previous study [65] where we determined the $[O_2]$ dependence of k_{ox} for iNOS to determine the 2nd order rate constant. In simulation, we also multiplied the observed oxygen binding rates to Fe^{II} intermediates by a factor of 2 to get a full air-saturated condition, assuming that the rate is proportional to $[O_2]$. The NADPH and chosen O_2 concentrations were kept constant during each simulation, to avoid secondary effects due to their exhaustion.

3. Results and discussion

3.1. Protein properties

Fig. 2 shows a cartoon of the chimeras we generated and used in our study. Purification yields were 38, 24, and 17 mg per liter of culture for WT chimera, V346I chimera, and S1412D chimera, respectively, these are all within the typical range seen when expressing mammalian NOS full-length enzymes. All three chimeras displayed Soret absorbance peaks at 398 nm in the presence of H_4B and Arg (Fig. 3), indicating they contained a five-coordinate high-spin heme iron as occurs in wild type iNOS when it has H_4B and Arg bound under similar conditions [18,34,42,49,60,66]. The chimeras bound imidazole to form a normal Soret peak with maxima at 428 nm, although imidazole binding may be sterically hindered in the V346I chimera. Addition of dithionite and CO to the chimeras generated ferrous–CO complexes with Soret absorbance at 444 nm (Fig. 3), again similar to wild-type NOS. These properties demonstrate that swapping the reductase domains, and introduction of the point mutations, did not significantly perturb substrate/cofactor binding, CaM response, or the electronic properties of the NOS heme in the chimeras.

Table 1
NO release and NADPH oxidation activities of the enzymes. Assays were run at 25 °C. Turnover number is expressed as moles of product formed per mole of NOS heme per min. Data are the mean and S.D. of three to four determinations. N.D., not determined; W.T., wild-type.

Enzymes	H_4B + Arg			H_4B + NOHA			H_4B + SEITU	Refs.
	NO release (min^{-1})	NADPH oxidation (min^{-1})	NADPH/NO	NO release (min^{-1})	NADPH oxidation (min^{-1})	NADPH/NO	NADPH oxidation (min^{-1})	
WT-iNOS	93 ± 1	160 ± 1	1.7	122 ± 2	117 ± 7	1.0	23 ± 1	This paper
WT-Chimera	119 ± 5	222 ± 3	1.9	157 ± 9	168 ± 5	1.1	39 ± 4	This paper
V346I iNOS	15 ± 1	59 ± 2	3.9	24 ± 1	36 ± 2	1.5	N.D.	[49]
V346I-Chimera	11 ± 0.3	91 ± 2	8.1	20 ± 1	116 ± 3	5.7	35 ± 3	This paper
S1412D-Chimera	107 ± 6	222 ± 3	2.1	168 ± 4	236 ± 1	1.4	59 ± 2	This paper

Please cite this article as: Z.-Q. Wang, et al., Engineering nitric oxide synthase chimeras to function as NO dioxygenases, J. Inorg. Biochem. (2016), http://dx.doi.org/10.1016/j.jinorgbio.2016.03.002

3.2. NO synthesis and NADPH oxidation

We measured steady-state NO synthesis activity (the NO release activity) and the associated NADPH oxidation at 25 °C, using Arg or the reaction intermediate NOHA as substrates. The results are given in Table 1. Compared to wild-type iNOS, the NO release activities of the WT and S1412D chimeras were 28% and 15% higher with Arg as substrate, and were 29% and 38% higher with NOHA as substrate, respectively. These increases are consistent with the predicted behavior of these two chimeras: Their nNOSred component should support a faster heme reduction (k_r) to iNOSoxy as compared to the iNOSred component in native iNOS, and this effect on k_r should enable these two chimeras to display a greater steady-state NO release rate (see Fig. 1). Indeed, the NADPH oxidation rates that accompanied NO synthesis by the WT and S1412D chimeras were increased compared to wild-type iNOS (Table 1). The ratio of NADPH oxidized per NO formed was similar between wild-type iNOS and the WT chimera, but was higher for the S1412D chimera (Table 1). Its increased ratio may reflect some increase in uncoupled NADPH oxidation that appears to be inherent in the S1412 nNOSred, as judged from the S1412D chimera having a higher NADPH oxidation rate when it was measured in the presence of S-ethyl-isothiourea (SEITU, Table 1), which is a substrate-competitive inhibitor that blocks iNOS heme reduction [67].

In comparison, the V346I chimera displayed 88% and 94% lower NO release activities with Arg or NOHA as substrates, respectively, relative to native iNOS (Table 1). A decrease was expected, because our previous work had shown that incorporating the V346I substitution alone into iNOS lowered its NO release activity by 79% [49] (Table 1). The V346I mutational effect on NO release activity was not related to poor substrate binding because the V346I substitution does not alter the substrate binding affinity [49]. NADPH oxidation by the V346I chimera when catalyzing Arg oxidation was only 45% slower than the rate seen in parent iNOS, and it's rate was similar to parent iNOS when it was catalyzing NOHA oxidation (Table 1). Thus, the V346I chimera had ratios of 8.1 or 5.7 NADPH oxidized per NO released with Arg or NOHA as substrates, respectively, which are considerably higher than ratios recorded for parent iNOS or for V346I iNOS (Table 1). The higher NADPH consumption of the V346I chimera, compared to its NO release, is consistent with the V346I chimera having an increased NO dioxygenase activity.

3.3. Kinetics of heme reduction

We utilized stopped-flow spectroscopy to determine the heme reduction rate (k_r) of the chimeras. Ferric enzymes containing Arg, H_4B, CaM and Ca^{2+} were rapidly mixed with excess NADPH in the presence of CO-saturated buffer under anaerobic conditions [26,30,59,68], and rate of heme reduction was determined as the rate of heme $Fe^{II}CO$ complex formation, as indicated by an absorbance increase at 444 nm. Fig. 4 contains kinetic traces from representative reactions that were run with each chimera and spectra are shown in the supplemental figure. The initial absorbance decrease at 444 nm that is seen in all cases was due to flavin reduction that takes place before electrons can transfer to the ferric heme [26,48,68–70]. All three chimeras exhibited a similar extent of heme reduction, that was also similar to parent iNOS [29,48,49,71], suggesting no large differences in the thermodynamics. The rates of absorbance change at 444 nm were fit to a biphasic equation, which gave estimated heme reduction rates of 1.9 ± 0.08, 1.8 ± 0.15 and 2.2 ± 0.05 s^{-1}, respectively, for the WT, V346I, and S1412D chimeras (Table 2).

The nNOSred component that was part of each chimera supported heme reduction rates (k_r) that were somewhat faster than the rates seen in the parent iNOS or in V346I iNOS (Table 2), thus achieving one of our protein engineering goals for the chimeras. Despite the k_r of the V346I chimera being 2.6 times faster than in V346I iNOS, the NO release rate of the V346I chimera (11 min^{-1}, Table 1) was 27% less than that for V346I iNOS (15 min^{-1}) [49]. This is in accord with the V346I chimera having a k_r/k_d ratio of 2.3 (see Table 2), which means that the increase in its heme reduction rate that is afforded by its nNOSred component should mainly increase shunting of the enzyme $Fe^{III}NO$ species into the futile cycle (see Fig. 1), and thus should have a negative overall effect on its NO release rate during the steady state.

Although the k_r values of the chimeras were all somewhat faster than in parent iNOS, they were still 40% to 60% slower than the k_r that is seen for nNOS, which ranges from 3 to 6 s^{-1} under the same experimental conditions [24,27,29,41,69] (Table 2). This difference was unexpected, because our previous work with an eNOSoxy/nNOSred chimera showed that the attached nNOSred component in that case supported the same heme reduction rate in eNOSoxy as is seen in nNOS [39]. The slower k_r we observed in our nNOSred/iNOSoxy chimeras is not likely due to a hindrance in CO binding in iNOSoxy, because CO binding to ferrous iNOSoxy is faster than the measured heme reduction rates [72]. We speculate that nNOSred may reduce the heme in the attached iNOSoxy more slowly because the iNOS heme has a lower midpoint potential than in nNOS [73], and/or because the iNOSoxy may have a docking site for the reductase domain that contains comparatively less charged residues available for docking when compared to the eNOSoxy or nNOSoxy surfaces [30]. These possibilities deserve further investigation. In any case, the slower than expected k_r that we achieved in our nNOSred/iNOSoxy chimeras likely compromises their capacities to act as NO dioxygenases, because the extent of enzyme partitioning into the futile (NO dioxygenase) cycle is directly related to the magnitude of k_r''' (see Fig. 1).

3.4. Nitrate and nitrite production

NO that is released into air-saturated water primarily oxidizes to nitrite, whereas the NO dioxygenase reaction converts NO to nitrate [49,55]. Thus, the nitrite to nitrate ratio can approximate what proportions of a NOS enzyme partition through the productive versus futile cycles, respectively, during catalysis. We measured the nitrate and nitrite formed in the reactions catalyzed by each chimera and wild-type iNOS. The WT and S1412D chimeras had nitrate:nitrite ratios similar to the ratio we obtained with parent iNOS, suggesting that they had a similar NO dioxygenase activity (Table 3). This is consistent with their having a less than expected increase in their k_r values (see Table 2), as discussed above, and with their measured ratios of the NADPH oxidized to NO released activities being only marginally greater than for wild-type iNOS (see Table 1). In comparison, the nitrate:nitrite product ratio of the V346I chimera was much higher and suggested it oxidized on average 4.5 NO for every NO it released, assuming that all the released NO went on to form nitrite. Because this ratio is higher than the 2.8 nitrate:nitrite released ratio that we observed for V346I iNOS in a similar study [49] (Table 3), it suggests that the 2.6 times faster heme reduction rate in the V346I chimera relative to V346I iNOS (Table 2) makes a significant contribution toward increasing the V346I chimera's NO dioxygenase activity. As noted above, this makes sense because the increase in k_r places the $Fe^{III}NO$ partition ratio (k_r'''/k_d) of the V346I chimera above unity, which then favors its entry into the futile cycle during steady-state catalysis (see Fig. 1).

The NO dioxygenase activity of iNOS can also involve its catalyzing the dioxygenation of NO that has been released into solution, if the NO concentration builds up sufficiently for it to bind to the iNOS heme [74]. Interestingly, V346I iNOS actually displays a diminished dioxygenase activity toward external NO relative to wild-type iNOS, because the V346I substitution restricts NO entrance into the iNOS heme pocket [49]. Thus, the greater NO dioxygenase activity that we see for the V346I chimera is likely due to its catalyzing an increased dioxygenation of the newly-formed NO within its heme pocket, and does not likely involve any increase in its dioxygenase activity toward external NO.

Please cite this article as: Z.-Q. Wang, et al., Engineering nitric oxide synthase chimeras to function as NO dioxygenases, J. Inorg. Biochem. (2016), http://dx.doi.org/10.1016/j.jinorgbio.2016.03.002

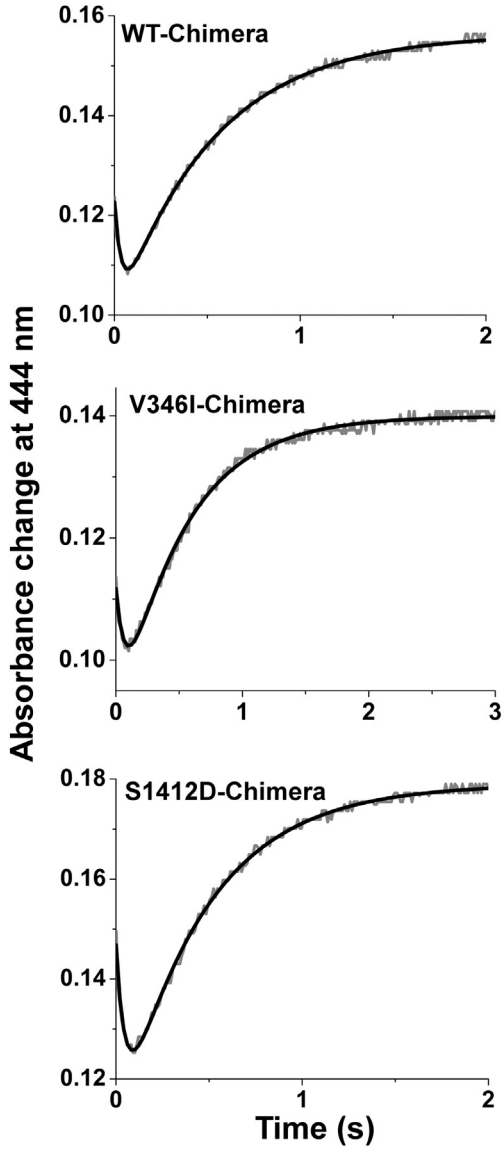

Fig. 4. Kinetics of heme reduction in the chimeric enzymes. Anaerobic solutions containing H_4B, Arg, $CaCl_2$ and CaM and ~10 μM ferric NOS protein were rapidly mixed with an anaerobic CO-saturated buffer solution containing 100 μM NADPH at 10 °C in a stopped flow spectrophotometer with diode array detection. Scans were recorded and heme reduction was followed by the formation of the ferrous–CO complex with Soret maximum at 444 nm. The lines of best fit are black.

3.5. Simulation of catalytic behaviors

We utilized the kinetic parameters listed in Table 4, which were derived from our measures at 10 °C and from our previous publications as noted in the Table, to run computer simulations of our global model for NOS catalysis as shown in Fig. 1 [18,24,29,45,49], in order to model the NO release activity, NADPH oxidation, and product ratios, as well as any changes in steady-state enzyme distribution, of the three chimeras relative to the parent iNOS. In addition, we measured the steady-state catalytic activities of the enzymes at 10 °C (Table 5), to obtain experimental measures that could be directly compared with the simulation results, which utilize kinetic parameters that were measured at 10 °C (i.e., the values in Table 5). The simulation results are valuable because they help to test our ideas about how the altered kinetic parameters in the chimeras may change their steady state activity outcomes (NO release & NADPH oxidation rates, NO to nitrate produced), particularly with regard to their having increased NO dioxygenase activity.

In our study, the "outcomes" (steady state catalytic activities and product ratios) showed a similar rank order among the enzymes when measured at 10 and 25 °C. This implies that temperature difference is not a major factor in projecting how the enzymes may behave at their physiologic temperature. Regarding a lack of large (5–10×) differences in some of our individual rate or activity measures among the chimeras, and the possibility of such smaller differences to influence outcomes: It is important to note that the outcomes (NO release activity, NADPH consumption, nitrate production) all rely on the blending of the individual measured rate parameters within the global catalytic model, and so relatively small differences among the rate parameters can in some cases have compounded effects on outcome, depending on how they blend in relation to one another. One good example is in how the ratio of the rate of $Fe^{III}NO$ reduction (k_r'") and the rate of $Fe^{III}NO$ dissociation (k_d) (i.e., k_r'"/k_d) determine the enzyme partitioning between the productive versus futile cycles. A 30% change in k_r'" would not have a big impact if the NOS k_d was 2 or 3 times faster than the original k_r'". However, in a situation where the original k_r'" and k_d are of similar speed, the same 30% increase in k_r'" would make it surpass the k_d, and thus would significantly shift the ratio for enzyme partitioning between the two cycles. Thus, more modest (30 to 200% changes) in any one of the rate parameters can still have significant impact on outcomes (and do so in our study), and thus can be informative for understanding the enzyme cycling and steady state behaviors in the chimeras. In fact, there are several similar studies where meaningful comparisons among NOS enzymes and mutants have been achieved, despite the overall change for any one rate parameter being fairly small [30,56,59].

Fig. 5 depicts the measured and simulated rates we obtained for steady-state NO release and NADPH consumption by iNOS and each of the three chimeras. The measured and simulated outcomes distribute in the same rank order: NO release rates were S1412D chimera, WT chimera ≥ iNOS ≫ V346I chimera, and NADPH oxidation rates were S1412D chimera, WT chimera > iNOS > V346I chimera. The magnitudes of each simulated and measured rate were well within a factor of two of one another. Thus, the simulations provided a reasonable match to the measured outcomes. The bottom panel of Fig. 5 compares the NADPH oxidized per NO released ratios of each enzyme, when derived from either the measured or simulated data in the upper and middle panels of Fig. 5. This analysis particularly distinguishes the V346I chimera for its poor NO release activity relative to its NADPH consumption, which is the expected behavior of a NOS enzyme that has become a predominant NO dioxygenase.

Table 2
Kinetic parameters for NOS enzymes and chimeras. Values of the k_r, k_{ox}, and k_d parameters were determined at 10 °C unless otherwise noted. k_r, rate of ferric heme reduction. k_d, dissociation rate of the ferric heme-NO complex. k_{ox}, rate of reaction between the ferrous heme-NO complex and approximately 140 μM O_2 (half air-saturated conditions). WT., wild-type.

NOS	heme reduction k_r (s^{-1})	$Fe^{III}NO$ dissociation k_d (s^{-1})	$Fe^{II}NO$ oxidation k_{ox} (s^{-1})	Refs.
WT-Chimera	1.9 ± 0.08	2.3 ± 0.1	3.1 ± 0.15	This paper, [49]
V346I-Chimera	1.8 ± 0.15	0.77 ± 0.03	1.8 ± 0.01	This paper, [49]
S1412D-Chimera	2.2 ± 0.05	2.3 ± 0.1	3.1 ± 0.15	This paper, [49]
V346I iNOS	0.69 ± 0.02	0.77 ± 0.03	1.8 ± 0.01	[49]
WT- iNOS	0.9–1.5	2	3	[29,41,49,73,74]
WT-nNOS	3–4	5	0.2	[24,29,41,69]
S1412D nNOS	5.4 ± 0.4	5	0.2	[27,29,50]

Please cite this article as: Z.-Q. Wang, et al., Engineering nitric oxide synthase chimeras to function as NO dioxygenases, J. Inorg. Biochem. (2016), http://dx.doi.org/10.1016/j.jinorgbio.2016.03.002

Table 3
Nitrite and nitrate production in NADPH-driven reaction at 37 °C. Reactions were run for 30 min prior to quenching as described under "Section 2." The values are the mean ± S.D. of three measurements.

NOS	NO_2^- produced (mol/mol NOS)	NO_3^- produced (mol/mol NOS)	NO_3^-/NO_2^-	Refs.
WT-iNOS	1572 ± 18	1409 ± 16	0.9	This paper
WT-Chimera	1853 ± 43	1848 ± 49	1.0	This paper
V346I-iNOS	2400	6800	2.8	[49]
V346I-Chimera	303 ± 11	1351 ± 21	4.5	This paper
S1412D-Chimera	1934 ± 32	1973 ± 16	1.0	This paper

Table 4
Rates used for the computer simulation.

			WT-iNOS	WT-Chimera	V346I-Chimera	S1412D-Chimera
k_1	$Fe^{III}(a) \rightarrow Fe^{II}(a)$	k_r	1.1	1.9	1.8	2.2
k_2	$Fe^{II}(a) (+ O_2) \rightarrow Fe^{II}O_2(a)$		106	106	31	106
k_3	$Fe^{II}O_2(a) \rightarrow Fe^{III}(b^*)$	k_{cat1}	12.5	12.5	3.7	12.5
k_4	$Fe^{III}(b^*) \rightarrow Fe^{III}(b)$	$k_{r'}$	1.1	1.9	1.8	2.2
k_5	$Fe^{III}(b) \rightarrow Fe^{II}(b)$	$k_{r''}$	1.1	1.9	1.8	2.2
k_6	$Fe^{II}(b) (+ O_2) \rightarrow Fe^{II}O_2(b)$		106	106	31	106
k_7	$Fe^{II}O_2(b) \rightarrow \mathbf{Fe^{III}NO}$	k_{cat2}	36.7	36.7	4.5	36.7
k_8	$Fe^{III}NO \rightarrow Fe^{III}(a) + NO$	k_d	2.0	2.3	0.8	2.3
k_9	$Fe^{III}NO \rightarrow Fe^{II}NO$	$k_{r'''}$	1.1	1.9	1.8	2.2
k_{10}	$Fe^{II}NO (+ O_2) \rightarrow Fe^{III}(a) + NO_x$	k_{ox}	4.5	4.65	2.7	4.65
k_{11}	$Fe^{II}NO \rightarrow Fe^{II}(a) + NO$		0.00006	0.00006	0.00006	0.00006
k_{12}	$Fe^{II}O_2(b) \rightarrow Fe^{III}(b)$		11.0	11.0	2.3	11.0
k_{13}	$Fe^{II}O_2(a) \rightarrow Fe^{III}(a)$		0.3	0.3	0.023	0.023

(a) Denotes L-Arg-bound enzyme; (b) denotes NOHA-bound enzyme; $Fe^{III}(b^*)$ indicates the ferric enzyme with NOHA and H_4B radical bound, see scheme in Fig. 1 for details. All values are in s^{-1}. For bimolecular reactions (k_2, k_6, k_{10}) the value used in the calculations is the product of the "actual" value and the concentration of oxygen, which is considered to remain constant during the reaction. For k_2 and k_6 the values used are the experimental values multiplied by 2 (assumes the rate is proportional to $[O_2]$, experimental values are determined in half air-saturated conditions). For k_{10} the values used are the experimentally determined values ×1.5 (based on observed oxygen dependence seen in Tejero et al. [65]. k_{11} values are interpolated from Salerno et al. paper [76]. k_{12} and k_{13} values are used from Wang et al. paper [49].

Fig. 6 informs on the measured and simulated NO dioxygenase activities of each enzyme, as judged from their nitrate versus nitrite productions in Table 3, and from their simulated nitrate to NO release ratios in Table 5, respectively. In both analyses, the V346I chimera is indicated to have ratios that indicate that its steady-state catalysis mainly occurs through the futile cycle (nitrate) versus productive (NO) pathway. It is unclear why the simulations indicate a lesser extent of futile cycling for the V346I chimera compared to the experimental estimate we derived from the nitrate and nitrite production, but in any case, they both indicate that this chimera has a predominant NO dioxygenase activity.

The simulations can also predict how each enzyme distributes among the five major enzyme species that form during steady-state catalysis (Table 6 and Fig. 7). In all cases, the simulations predict that the ferric form of each enzyme should remain the predominant species during the steady state, but also indicate that its proportion will be diminished in all three chimeras relative to native iNOS, and will be diminished to the greatest extent in the V346I chimera. The loss of the ferric form is counterbalanced by increased buildup of the other enzyme species. In particular, all three chimeras should have increased buildup of their $Fe^{II}NO$ species, which is consistent with their having increased partitioning into the futile cycle due to their faster k_r values compared to iNOS, and in the case of the V346I chimera, is also consistent with its having a slower k_d. The predicted greater buildup of the $Fe^{II}O_2$ species in the V346I chimera can be justified from it's having a faster heme reduction (k_r, k_r') than iNOS, which speeds formation of the $Fe^{II}O_2$ species, coupled with it's having slower k_{cat1} and k_{cat2} rates, which prolongs the lifetime of the $Fe^{II}O_2$ species. Consequently, the V346I chimera should be more susceptible to uncoupling, due to increased partitioning of the $Fe^{II}O_2$ species to Fe^{III} and superoxide [49] (see Fig. 1). This process in turn may contribute to the higher NADPH oxidation rate we see for the V346I chimera, beyond the level that is needed to explain its increased NO dioxygenase activity.

The impact of replacing the natural iNOSred with nNOSred in the V346I chimera can be further appreciated by comparing the simulated enzyme distributions of the chimera versus V346I iNOS [49]. The relatively faster k_r in the V346I chimera is expected to cause more accumulation of the $Fe^{II}NO$ species during steady-state NO synthesis, due to its causing more enzyme to partition into the futile cycle. The simulations support this notion, predicting 12.5% of the V346I chimera would accumulate as its $Fe^{II}NO$ complex (Table 6), versus only 4.5% predicted for V346I iNOS [49]. Because the $Fe^{II}NO$ complex is actually an inhibited

Table 5
Measured and simulated rates at 10 °C.

Enzymes	H4B + Arg + CaM			H4B + Arg -CaM	Simulation data			
	NO release (min^{-1})	NADPH oxidation (min^{-1})	NADPH Ox/NO release	NADPH oxidation (min^{-1})	NO release (min^{-1})	NADPH oxidation (min^{-1})	NADPH Ox/NO release	NOx/NO
WT- iNOS	27 ± 2	42 ± 4	1.55	13 ± 1	18	46	2.5	0.68
WT-Chimera	36 ± 3	66 ± 3.5	1.8	12 ± 0.8	22	64	2.9	0.93
V346I-Chimera	2.5 ± 0.2	22 ± 2.8	8.8	3.5 ± 0.4	5.2	34	6.5	2.17
S1412D-Chimera	43 ± 2	72 ± 7	1.7	10 ± 1	21	58	2.8	0.96

Please cite this article as: Z.-Q. Wang, et al., Engineering nitric oxide synthase chimeras to function as NO dioxygenases, J. Inorg. Biochem. (2016), http://dx.doi.org/10.1016/j.jinorgbio.2016.03.002

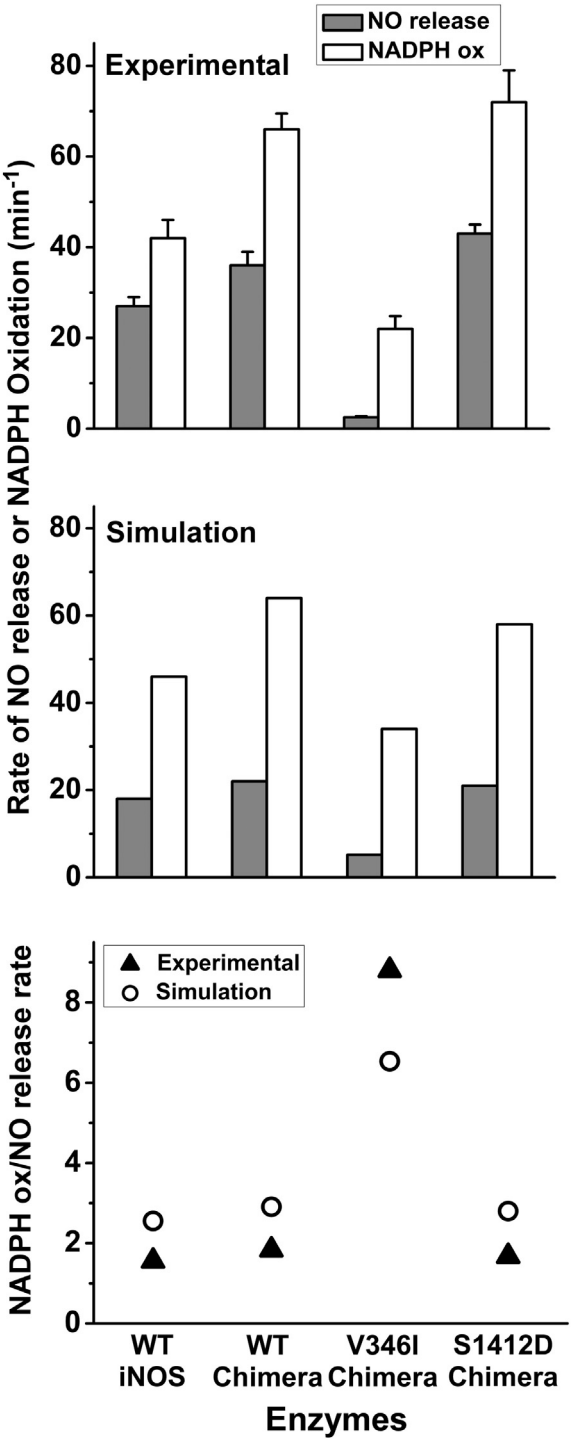

Fig. 5. Comparison of experimental and simulated NO release and NADPH consumption rates for the different NOS enzymes. *Upper panel* — Bar graph showing the measured NO release rates and NADPH consumption rates for each enzyme at 10 °C. *Middle panel* — Bar graph showing simulated NO release and corresponding NADPH oxidation rates for each enzyme at 10 °C. *Lower panel* — The ratio of NADPH consumed per NO released for each enzyme in the experimental and simulated conditions.

(or poisoned) form of NOS enzymes, its increased buildup will slow overall enzyme cycling, decrease steady-state activity, and will increase the importance of the k_{ox} parameter and its associated NO dioxygenase reaction in determining the behavior of enzyme molecules during catalysis.

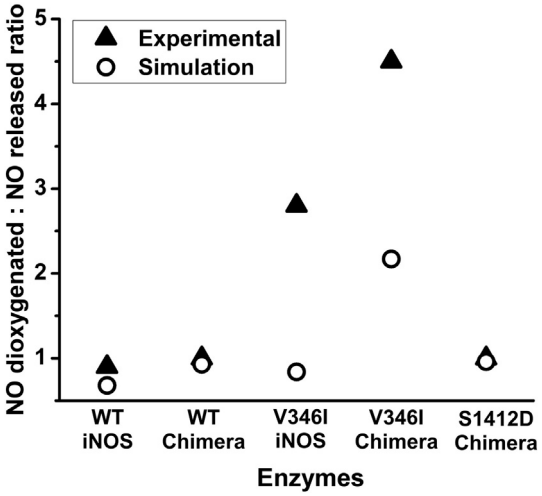

Fig. 6. NO dioxygenase activities of different NOS enzymes. The ratio of NO deoxygenated per NO released was determined as the ratio of nitrate to nitrite formed by each enzyme (NO_3^-/NO_2^-) from reactions described in Table 3, and from the ratio of nitrate formed per NO released (NOx/NO) from the simulation data in Table 5.

4. Conclusions

In our study we aimed to engineer iNOS proteins to function primarily as NO dioxygenases, by altering structural features that were known to impact two kinetic parameters (k_r, and k_d) that help to determine the extent of NOS enzyme cycling between its productive (NO-releasing) and futile (NO dioxygenase) pathways. We succeeded in creating one NOS chimera with predominant NO dioxygenase function relative to its NO release. Our work provides a better understanding of how distinct protein structures or structural features regulate key kinetic parameters in NOS enzymes, and how interplay between these parameters can tune and balance the inherent NO releasing and NO dioxygenase activities that are present in all NOS enzymes. Besides adding to the general fundamental understanding, our study provides a template for rational design of NOS enzymes in order to regulate or change their functions in various biological settings [75].

Supplementary data to this article can be found online at http://dx.doi.org/10.1016/j.jinorgbio.2016.03.002.

Acknowledgments

This work was supported by the National Institutes of Health grants GM51491 and CA53914 (D. J. S.), the American Heart Association Beginning Grant-in-aid 0565297B (Z-Q. W.), KSU Farris Innovation Award (Z-Q. W.), KSU Faculty Professional Improvement Leave Award (Z-Q. W.), the American Heart Association Beginning Grant-in-aid 0365175B (C.C.W), and SIUE See Grants for Transitional and Exploratory Projects (C.C. W).

Table 6
Simulations of enzyme distribution during steady-state catalysis. Values were obtained by computer simulation of the global kinetic model described in "Section 2" and Fig. 1. WT, wild type.

	WT-iNOS	WT-Chimera	V346I-Chimera	S1412D-Chimera	V346I-iNOS
Fe^{III}%	82.3	76.5	59.7	73.9	75.1
$Fe^{II}NO$%	3.1	7.0	10.1	8.4	5.6
Fe^{II}%	0.8	1.0	2.6	1.1	1.3
$Fe^{II}O_2$%	3.6	4.9	15.5	5.3	7.7
$Fe^{III}NO$%	10.2	10.6	12.1	11.3	10.3

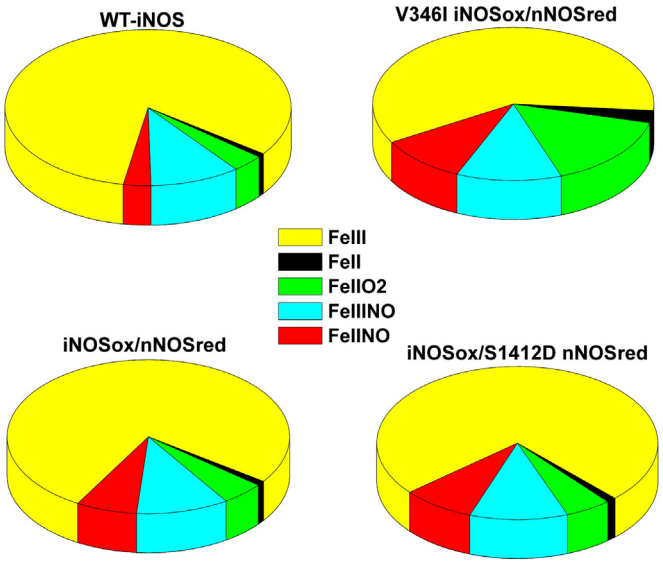

Fig. 7. Simulated enzyme distribution patterns during steady state NO synthesis. Distributions of the five major enzyme species are indicated for WT-iNOS and the three chimeras.

References

[1] M.G. Campbell, B.C. Smith, C.S. Potter, B. Carragher, M.A. Marletta, Proc. Natl. Acad. Sci. U. S. A. 111 (2014) E3614–E3623.
[2] S. Daff, Nitric Oxide 23 (2010) 1–11.
[3] C. Feng, Coord. Chem. Rev. 256 (2012) 393–411.
[4] T.L. Poulos, Chem. Rev. 114 (2014) 3919–3962.
[5] D.J. Stuehr, Annu. Rev. Pharmacol. Toxicol. 37 (1997) 339–359.
[6] D.J. Stuehr, Biochim. Biophys. Acta 1411 (1999) 217–230.
[7] B.S. Masters, K. McMillan, E.A. Sheta, J.S. Nishimura, L.J. Roman, P. Martasek, FASEB J. 10 (1996) 552–558.
[8] U. Siddhanta, C. Wu, H.M. bu-Soud, J. Zhang, D.K. Ghosh, D.J. Stuehr, J. Biol. Chem. 271 (1996) 7309–7312.
[9] B.R. Crane, A.S. Arvai, D.K. Ghosh, C. Wu, E.D. Getzoff, D.J. Stuehr, J.A. Tainer, Science 279 (1998) 2121–2126.
[10] T.O. Fischmann, A. Hruza, X.D. Niu, J.D. Fossetta, C.A. Lunn, E. Dolphin, A.J. Prongay, P. Reichert, D.J. Lundell, S.K. Narula, P.C. Weber, Nat. Struct. Biol. 6 (1999) 233–242.
[11] A.C. Gorren, M. Sorlie, K.K. Andersson, S. Marchal, R. Lange, B. Mayer, Methods Enzymol. 396 (2005) 456–466.
[12] R. Gachhui, A. Presta, D.F. Bentley, H.M. Abu-Soud, R. McArthur, G. Brudvig, D.K. Ghosh, D.J. Stuehr, J. Biol. Chem. 271 (1996) 20594–20602.
[13] E.D. Garcin, C.M. Bruns, S.J. Lloyd, D.J. Hosfield, M. Tiso, R. Gachhui, D.J. Stuehr, J.A. Tainer, E.D. Getzoff, J. Biol. Chem. 279 (2004) 37918–37927.
[14] M.M. Haque, M. Bayachou, J. Tejero, C.T. Kenney, N.M. Pearl, S.C. Im, L. Waskell, D.J. Stuehr, FEBS J. 281 (2014) 5325–5340.
[15] D.J. Stuehr, J. Tejero, M.M. Haque, FEBS J. 276 (2009) 3959–3974.
[16] H. Li, T.L. Poulos, J. Inorg. Biochem. 99 (2005) 293–305.
[17] B.C. Smith, E.S. Underbakke, D.W. Kulp, W.R. Schief, M.A. Marletta, Proc. Natl. Acad. Sci. U. S. A. 110 (2013) E3577–E3586.
[18] L. Hannibal, R.C. Page, M.M. Haque, K. Bolisetty, Z. Yu, S. Misra, D.J. Stuehr, Biochem. J. (2015).
[19] C.C. Wei, Z.Q. Wang, Q. Wang, A.L. Meade, C. Hemann, R. Hille, D.J. Stuehr, J. Biol. Chem. 276 (2001) 315–319.
[20] C.C. Wei, Z.Q. Wang, C. Hemann, R. Hille, D.J. Stuehr, J. Biol. Chem. 278 (2003) 46668–46673.
[21] J. Tejero, D. Stuehr, IUBMB Life 65 (2013) 358–365.
[22] E. Butt, M. Bernhardt, A. Smolenski, P. Kotsonis, L.G. Frohlich, A. Sickmann, H.E. Meyer, S.M. Lohmann, H.H. Schmidt, J. Biol. Chem. 275 (2000) 5179–5187.
[23] M.M. Haque, K. Panda, J. Tejero, K.S. Aulak, M.A. Fadlalla, A.T. Mustovich, D.J. Stuehr, Proc. Natl. Acad. Sci. U. S. A. 104 (2007) 9254–9259.
[24] M.M. Haque, J. Tejero, M. Bayachou, Z.Q. Wang, M. Fadlalla, D.J. Stuehr, FEBS J. 280 (2013) 4439–4453.
[25] M.B. Harris, H. Ju, V.J. Venema, H. Liang, R. Zou, B.J. Michell, Z.P. Chen, B.E. Kemp, R.C. Venema, J. Biol. Chem. 276 (2001) 16587–16591.
[26] K. Panda, M.M. Haque, E.D. Garcin-Hosfield, D. Durra, E.D. Getzoff, D.J. Stuehr, J. Biol. Chem. 281 (2006) 36819–36827.
[27] J. Santolini, S. Adak, C.M. Curran, D.J. Stuehr, J. Biol. Chem. 276 (2001) 1233–1243.
[28] J. Santolini, M. Roman, D.J. Stuehr, T.A. Mattioli, Biochemistry 45 (2006) 1480–1489.
[29] D.J. Stuehr, J. Santolini, Z.Q. Wang, C.C. Wei, S. Adak, J. Biol. Chem. 279 (2004) 36167–36170.
[30] J. Tejero, L. Hannibal, A. Mustovich, D.J. Stuehr, J. Biol. Chem. 285 (2010) 27232–27240.
[31] W.K. Alderton, C.E. Cooper, R.G. Knowles, Biochem. J. 357 (2001) 593–615.
[32] K. Bian, F. Murad, Front. Biosci. 8 (d264–78) (2003) d264–d278.
[33] R.K. Cross, K.T. Wilson, Inflamm. Bowel Dis. 9 (2003) 179–189.
[34] S. Ghosh, D. Wolan, S. Adak, B.R. Crane, N.S. Kwon, J.A. Tainer, E.D. Getzoff, D.J. Stuehr, J. Biol. Chem. 274 (1999) 24100–24112.
[35] S. Ghosh, S.C. Erzurum, Drug Discov. Today Dis. Mech. 9 (2012) e89–e94.
[36] W.C. Sessa, Mem. Inst. Oswaldo Cruz 100 (Suppl. 1) (2005) 15–18.
[37] W.C. Sessa, Lancet Oncol. 8 (2007) 88–89.
[38] H.M. Abu-Soud, K. Ichimori, A. Presta, D.J. Stuehr, J. Biol. Chem. 275 (2000) 17349–17357.
[39] S. Adak, K.S. Aulak, D.J. Stuehr, J. Biol. Chem. 276 (2001) 23246–23252.
[40] R.T. Miller, P. Martasek, T. Omura, B.S.S. Masters, Biochem. Biophys. Res. Commun. 265 (1999) 184–188.
[41] J. Santolini, A.L. Meade, D.J. Stuehr, J. Biol. Chem. 276 (2001) 48887–48898.
[42] J. Tejero, A. Biswas, Z.Q. Wang, R.C. Page, M.M. Haque, C. Hemann, J.L. Zweier, S. Misra, D.J. Stuehr, J. Biol. Chem. 283 (2008) 33498–33507.
[43] Z.Q. Wang, C.C. Wei, S. Ghosh, A.L. Meade, C. Hemann, R. Hille, D.J. Stuehr, Biochemistry 40 (2001) 12819–12825.
[44] C.C. Wei, B.R. Crane, D.J. Stuehr, Chem. Rev. 103 (2003) 2365–2383.
[45] J. Tejero, A. Biswas, M.M. Haque, Z.Q. Wang, C. Hemann, C.L. Varnado, Z. Novince, R. Hille, D.C. Goodwin, D.J. Stuehr, Biochem. J. 433 (2011) 163–174.
[46] S. Adak, Q. Wang, D.J. Stuehr, J. Biol. Chem. 275 (2000) 33554–33561.
[47] C.R. Nishida, P.R. Ortiz de Montellano, J. Biol. Chem. 273 (1998) 5566–5571.
[48] Z.Q. Wang, C.C. Wei, J. Santolini, K. Panda, Q. Wang, D.J. Stuehr, Biochemistry 44 (2005) 4676–4690.
[49] Z.Q. Wang, C.C. Wei, D.J. Stuehr, J. Inorg. Biochem. 104 (2010) 349–356.
[50] S. Adak, J. Santolini, S. Tikunova, Q. Wang, J.D. Johnson, D.J. Stuehr, J. Biol. Chem. 276 (2001) 1244–1252.
[51] R. Kar, D.L. Kellogg III, L.J. Roman, Biochem. Biophys. Res. Commun. 459 (2015) 393–397.
[52] P.I. Nedvetsky, W.C. Sessa, H.H. Schmidt, Proc. Natl. Acad. Sci. U. S. A. 99 (2002) 16510–16512.
[53] L.J. Roman, P. Martasek, B.S. Masters, Chem. Rev. 102 (2002) 1179–1190.
[54] Z.Q. Wang, C.C. Wei, M. Sharma, K. Pant, B.R. Crane, D.J. Stuehr, J. Biol. Chem. 279 (2004) 19018–19025.
[55] E. Beaumont, J.C. Lambry, Z.Q. Wang, D.J. Stuehr, J.L. Martin, A. Slama-Schwok, Biochemistry 46 (2007) 13533–13540.
[56] M.M. Haque, M. Fadlalla, Z.Q. Wang, S.S. Ray, K. Panda, D.J. Stuehr, J. Biol. Chem. 284 (2009) 19237–19247.
[57] M.M. Haque, M. Bayachou, M.A. Fadlalla, D. Durra, D.J. Stuehr, Biochem. J. 450 (2013) 607–617.
[58] M.M. Haque, M.A. Fadlalla, K.S. Aulak, A. Ghosh, D. Durra, D.J. Stuehr, J. Biol. Chem. 287 (2012) 30105–30116.
[59] J. Tejero, M.M. Haque, D. Durra, D.J. Stuehr, J. Biol. Chem. 285 (2010) 25941–25949.
[60] Z.Q. Wang, J. Tejero, C.C. Wei, M.M. Haque, J. Santolini, M. Fadlalla, A. Biswas, D.J. Stuehr, J. Inorg. Biochem. 108 (2012) 203–215.
[61] D.J. Stuehr, M. Ikeda-Saito, J. Biol. Chem. 267 (1992) 20547–20550.
[62] S. Adak, C. Crooks, Q. Wang, B.R. Crane, J.A. Tainer, E.D. Getzoff, D.J. Stuehr, J. Biol. Chem. 274 (1999) 26907–26911.
[63] S. Adak, K.S. Aulak, D.J. Stuehr, J. Biol. Chem. 277 (2002) 16167–16171.
[64] Z.Q. Wang, R.J. Lawson, M.R. Buddha, C.C. Wei, B.R. Crane, A.W. Munro, D.J. Stuehr, J. Biol. Chem. 282 (2007) 2196–2202.
[65] J. Tejero, J. Santolini, D.J. Stuehr, FEBS J. 276 (2009) 4505–4514.
[66] D.K. Ghosh, C. Wu, E. Pitters, M. Moloney, E.R. Werner, B. Mayer, D.J. Stuehr, Biochemistry 36 (1997) 10609–10619.
[67] H.M. Abu-Soud, P.L. Feldman, P. Clark, D.J. Stuehr, J. Biol. Chem. 269 (1994) 32318–32326.
[68] M.M. Haque, C. Kenney, J. Tejero, D.J. Stuehr, FEBS J. 278 (2011) 4055–4069.
[69] H.M. Abu-Soud, J. Wang, D.L. Rousseau, J.M. Fukuto, L.J. Ignarro, D.J. Stuehr, J. Biol. Chem. 270 (1995) 22997–23006.
[70] S. Adak, Q. Wang, D.J. Stuehr, J. Biol. Chem. 275 (2000) 17434–17439.
[71] A. Presta, U. Siddhanta, C. Wu, N. Sennequier, L. Huang, H.M. Abu-Soud, S. Erzurum, D.J. Stuehr, Biochemistry 37 (1998) 298–310.
[72] H.M. Abu-Soud, C. Wu, D.K. Ghosh, D.J. Stuehr, Biochemistry 37 (1998) 3777–3786.
[73] A. Presta, A.M. Weber-Main, M.T. Stankovich, D. Stuehr, J. Am. Chem. Soc. 120 (1998) 9460–9465.
[74] H.M. Abu-Soud, K. Ichimori, H. Nakazawa, D.J. Stuehr, Biochemistry 40 (2001) 6876–6881.
[75] B.R. Crane, Biochem. Soc. Trans. 36 (2008) 1149–1154.
[76] J.C. Salerno, FEBS Lett. 582 (2008) 1395–1399.

Please cite this article as: Z.-Q. Wang, et al., Engineering nitric oxide synthase chimeras to function as NO dioxygenases, J. Inorg. Biochem. (2016), http://dx.doi.org/10.1016/j.jinorgbio.2016.03.002